A saturation-balancing control method for enhancing dynamic vehicle stability

Justin Sill and Beshah Ayalew*

Clemson University International Centre for Automotive Research,
4 Research Dr., 342 CGEC,
Greenville, SC 29607, USA
E-mail: jsill@clemson.edu
E-mail: beshah@clemson.edu
*Corresponding author

Abstract: This paper proposes a vehicle stability control method that quantifies and uses the level of lateral force saturation on each axle of a vehicle. The magnitude of the saturation is determined from on-line estimated nonlinear lateral tire forces and their linear projections. Once known, saturation levels are employed in a saturation balancing control structure that biases the drive torque to either the front or rear axles/wheels. The control structure avoids the need for an explicit reference model to generate target responses. The benefits of the proposed approach are demonstrated considering a nominally unstable vehicle in an extreme obstacle avoidance manoeuvre.

Keywords: VSC; vehicle stability control; saturation balancing; tyre force estimation; axle saturation level; independent drive; torque biasing.

Reference to this paper should be made as follows: Sill, J. and Ayalew, B. (2013) 'A saturation-balancing control method for enhancing dynamic vehicle stability', *Int. J. Vehicle Design*, Vol. 61, Nos. 1/2/3/4, pp.47–66.

Biographical notes: Justin Sill is a PhD Candidate in Automotive Engineering at the Clemson University-International Center for Automotive Research. He earned his MS and BS in Mechanical Engineering from Clemson University. He was a Research Assistant and a Graduate Teaching Assistant at Clemson. He then worked at Goodyear Tire & Rubber Company as a Vehicle Dynamics Engineer for more than three years before returning to graduate school for his doctoral work. His research interests and expertise are in modelling and control of dynamic systems, and track testing and modelling of vehicle/tyre performance. He is a member of ASME and SAE.

Beshah Ayalew is an Assistant Professor at the Clemson University-International Center for Automotive Research. He received his MS (2000) and PhD (2005) in Mechanical Engineering from Penn State University and his BS (1997), also in Mechanical Engineering, from Addis Ababa University, Ethiopia. He is a recipient of the NSF CAREER Award (2011) and the Penn State Alumni Association Dissertation Award (2005). His research interests lie in the area of dynamic systems modelling and control with a focus in distributed parameter process control, Vehicle Dynamics Control (VDC) and hydraulic/electric hybrid drive trains. He is a member of the ASME, IEEE and SAE.

1 Introduction

Vehicle Stability Control (VSC) systems have widely been shown to reduce accidents by minimising driver's loss of control during aggressive emergency manoeuvres. VSC systems manipulate one or more of the front or rear steering inputs, the traction or braking inputs, or the tyre vertical loads to favourably influence the forces and moments generated at the tyre–ground interface that in turn affect the lateral and yaw dynamics of the vehicle. The magnitude and direction of control intervention is often determined by calculating deviations from reference/desired vehicle responses such as its yaw rate or lateral acceleration.

The most common VSC (also referred to as Vehicle Dynamics Control (VDC)) systems available on the market today are brake-based systems, which extend the functionality of mature hardware technology available for Anti-lock Braking (ABS) and traction control systems. These systems facilitate differential (left-to-right) braking on either the front or rear axle to generate a corrective yaw moment on the vehicle for stabilisation or for accommodating driver intentions (Ghoneim et al., 2000; Rajamani, 2006; Tseng et al., 1999; Zanten, 2000). In addition to brake-based systems, VSC can be accomplished by active front/rear steering (Falcone et al., 2007a, 2007b, 2008). It can also be achieved by utilising active suspension components, such as active/semi-active dampers to change tyre loads (Hac and Bodie, 2002). Finally, VSC can also be achieved using active differentials/transaxles or independent axle/wheel drives to manage or redistribute traction forces for vehicle course corrections (Esmailzadeh et al., 2002; Goodarzi and Esmailzadeh, 2007; Karogal and Ayalew, 2009; Osborn and Shim, 2004; Piyabongkarn et al., 2007; Gradu, 2003; Mohan and Sharma, 2006). The implementation of these alternative, non-brake-based VSC systems is more likely to increase in advanced technology vehicles because of certain design benefits. For example, some of these systems help achieve a high degree of manoeuvrability at low speeds (active steering, active differentials/transaxles and independent drives), improve handling and ride (active suspensions), and have benefits of packaging convenience (independent drives) for some applications such as wheeled military vehicles.

This paper presents an advanced VSC strategy that is ideally suited for vehicles with torque biasing or independent drive architectures that deliver power individually to each axle or wheel of the vehicle. The core of the proposed VSC strategy is based on identifying the force generation capabilities or saturation levels of the individual axles or wheels on the vehicle and using this information for maintaining the lateral stability of the vehicle. The strategy is motivated by the possibility of applying traction and braking torques (with regenerative braking) at the individual wheels or axles of the vehicle with independent drive or torque-biasing systems. Independent drive systems can be readily configured for emerging power trains in series or parallel electric hybrids, fuel-cell or battery-powered electrics or hydraulic-hybrid vehicles. With these systems and the proposed VSC strategy, there is the possibility of enhancing stability and safety while maintaining the efficiency benefits of these systems and preserving driver intentions.

The proposed VSC strategy relies on the estimation of the available lateral and longitudinal force capacity for each axle of the vehicle from available sensors standard on current VSC systems. These sensors include an angular rate sensor for yaw rate, accelerometers for lateral and longitudinal accelerations, and ABS sensors for individual

wheel-spins. There are a number of previous research efforts that have addressed the estimation of tyre forces and axle slip angles. Perhaps the most common interest has been in the estimation of longitudinal and vertical forces for the purposes of obtaining tyre/road friction coefficients. The level of available adhesion is of importance to traction control, ABS and VSC systems (Tseng et al., 1999; Kim, 2010; Kim and Kim, 2007; Ray, 1995, 1997; Hongyan et al., 2009; Limroth, 2009). Vertical tyre forces (or normal loads) may be estimated by combining static weight distributions and perturbations owing to lateral/longitudinal accelerations of the vehicle body and effects of front/rear roll stiffness and damping distributions. Longitudinal tyre forces can be estimated using the known applied torque and wheel speed sensor signals of the vehicle, through direct inversion of tyre/wheel dynamics (Limroth, 2009) or using observer-based methods (Hongyan et al., 2009; Wanki et al., 2009) or extended Kalman filters (Kim, 2009; Kim and Kim, 2007; Ray, 1995, 1997).

The estimation of axle lateral forces have been important to recent vehicle dynamics research and are usually coupled with axle slip angle approximations to indirectly characterise the tyre behaviour that affects the lateral dynamics of the vehicle (Kim, 2007; Ray, 1995, 1997; Limroth, 2009; Fukada, 1999; Kim, 2009). The axle lateral forces can be estimated from the lateral acceleration and yaw rate sensors through an inversion of a single-track two Degree of Freedom (DOF) handling model (Limroth, 2009; Fukada, 1999), an observer (Wanki et al., 2009), or a Kalman filter (Kim, 2009; Kim and Kim, 2007; Ray, 1995, 1997; Kim, 2009). The axle slip angles may be calculated from an estimate of lateral velocity, which is most often achieved by using observers. These estimation efforts have been used in brake-based VSC algorithms (Kim, 2007; Limroth, 2009; Fukada, 1999; Kim, 2009), but can easily be employed in other VSC schemes like the one proposed in this paper for independent or torque-biasing drives.

This research paper addresses the monitoring and management of axle saturation levels for the purposes of VSC. Axle saturation will be explicitly estimated and quantified using established tyre force estimation schemes. A VSC structure is then set up to use the identified saturation levels and attempt to rebalance them among the front and rear axles of the vehicle in a manner that corrects understeer and oversteer. Interpretations will be given to the resulting control structure by comparing it against common model-reference VSC systems that use yaw-rate error feedback. While the proposed VSC approach is envisaged to be particularly suited for drive trains featuring independent per-axle and per-wheel drives or torque biasing/vectoring systems, the saturation balancing approach could also be adopted for use with brake-based VSC actuation systems. In this paper, we focus primarily on the independent or torque-biasing per-axle drive applications and merely highlight the opportunities and challenges for a per-wheel application of the proposed method.

The rest of the paper is organised as follows. Section 2 introduces the definition of axle saturation quantities adopted for this work. The details of the 7 DOF vehicle model adopted for the analysis in this paper are postponed to the Appendix. Section 3 details the motivation, interpretation and implementation of the proposed axle saturation balancing control method. Section 4 provides some demonstrative results illustrating the performance of the proposed method. Section 5 summarises the conclusions of the work and motivates future research, including a brief discussion on the possible application of the method to a per-wheel saturation balancing control system.

2 Determination of axle saturation

The determination of the saturation levels of the lateral forces at each of the front and rear axles requires some way of estimating tyre-ground forces. For this purpose, a rigid vehicle-handling model, such as the one shown in Figure 1, can be used as a starting point. The definitions of the various force, angle and speed variables shown in Figure 1 are standard and are described in the nomenclature list. The equations of motion derived from this 7 DOF model are also quite standard and are given in summarised form in Appendix A. The model is subsequently reduced to the usual 2 DOF (bicycle) model consisting of the lateral and yaw equations for the purposes of estimating the lateral tyre-ground forces.

Figure 1 Schematic of vehicle dynamics model (see online version for colours)

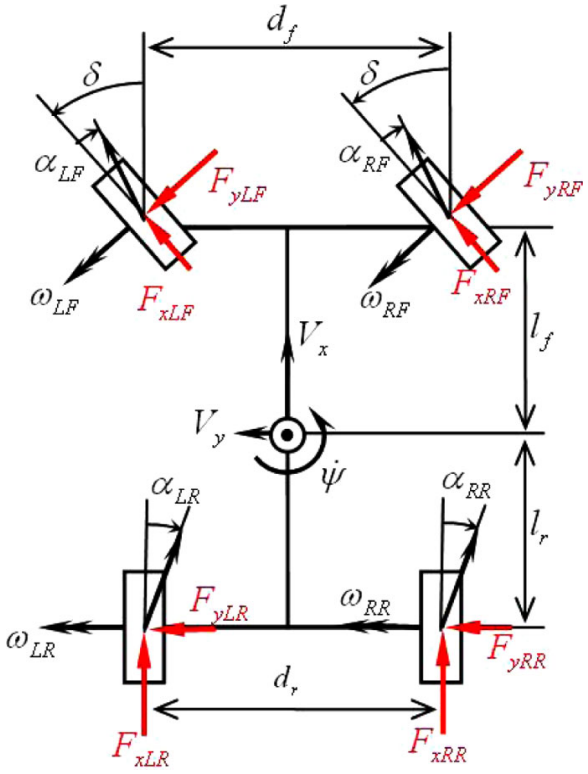

The front and rear lateral forces can be determined by inverting the bicycle handling model given measured lateral acceleration, yaw rate and steering angle signals. This approach has been taken in previous works (Ray, 1995, 1997; Limroth, 2009; Wanki et al., 2009; Fukada, 1999) where the per-axle lateral forces are estimated from variants of the equation

$$\begin{Bmatrix} \hat{F}_{yF} \\ \hat{F}_{yR} \end{Bmatrix} = \begin{bmatrix} \cos\delta & 1 \\ l_f \cos\delta & -l_r \end{bmatrix}^{-1} \left\{ \begin{bmatrix} mA_y \\ I_{zz} \dfrac{\mathrm{d}\dot{\psi}}{\mathrm{d}t} \end{bmatrix} - \hat{M}_x \right\} \tag{1}$$

where the variables with hats denote estimates, and

$$\hat{M}_x = \begin{bmatrix} \sin\delta & \sin\delta & 0 & 0 \\ l_f \sin\delta - \frac{d_f}{2}\cos\delta & l_f \sin\delta + \frac{d_f}{2}\cos\delta & -\frac{d_r}{2} & \frac{d_r}{2} \end{bmatrix} \begin{bmatrix} \hat{F}_{xLF} \\ \hat{F}_{xRF} \\ \hat{F}_{xLR} \\ \hat{F}_{xRR} \end{bmatrix}$$

In this work, the latter term is added to correct for the contribution of the longitudinal forces on the lateral dynamics (from equations (A.2) and (A.3)). This correction uses estimates of the longitudinal forces. There are several approaches for estimating longitudinal tyre forces using the controlled torque inputs and the speed sensors for each wheel. These methods range from a simple method that corrects for wheel rotational dynamics through direct differentiation of wheel speed sensor signals, to more advanced observer-based methods (Hongyan et al., 2009; Wanki et al., 2009). Here, for our purposes, we use the simple method for longitudinal force estimation

$$\hat{F}_{xi} = \left(T_i - I_w \frac{\mathrm{d}\omega_i}{\mathrm{d}t} \right) \Big/ R_w \tag{2}$$

where ω_i is the measured wheel speed, T_i is the applied torque and I_w and R_w are the tyre/wheel inertia and effective tyre radius, respectively.

Axle slip angles can be determined through an observer (or Kalman filter) by estimating lateral velocity from the lateral acceleration, longitudinal velocity and yaw rate sensors. For example, lateral velocity estimation can be set up as (Tseng et al., 1999; Limroth, 2009):

$$\frac{\mathrm{d}}{\mathrm{d}t}\hat{V}_y = \hat{A}_y - \dot{\psi} V_x + K_y (A_y - \hat{A}_y) \tag{3}$$

where $\hat{A}_y = \left(\hat{F}_{yF} + \hat{F}_{yR} \right) / M$ and $\dot{\psi}, V_x,$ and A_y are the measured yaw rate, speed and lateral acceleration of the vehicle, while K_y is an observer gain. The estimated axle slip angles can then be obtained from the kinematic relations:

$$\hat{\alpha}_F = \tan^{-1}\left(\frac{\hat{V}_y + l_f \dot{\psi}}{V_x} \right) - \delta \tag{4}$$

$$\hat{\alpha}_R = \tan^{-1}\left(\frac{\hat{V}_y - l_r \dot{\psi}}{V_x} \right) \tag{5}$$

Knowing estimates of the axle lateral forces and slip angles at each instant, a definition of the saturation level of the axle, α_{sat}, can be given using the illustration in Figure 2.

Figure 2 Definition of axle saturation (see online version for colours)

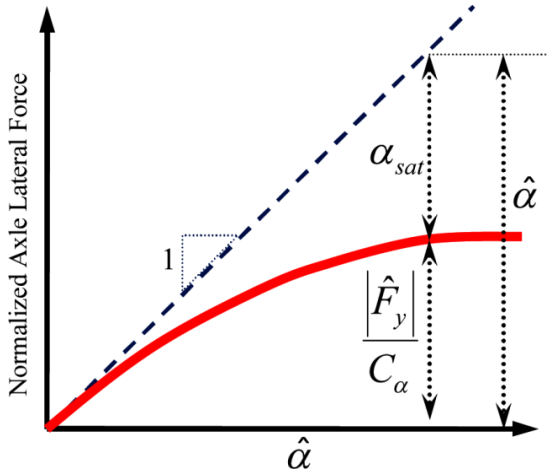

Assuming that the axle cornering stiffness is a known constant, the axle saturation can be defined as the difference between the normalised estimate of the non-linear axle lateral force (which has the dimensions of slip angle) and the prevailing estimated slip angle:

$$\alpha_{\text{sat}} = \hat{\alpha} - \frac{\hat{F}_y}{C_\alpha} \tag{6}$$

The axle saturation defined by equation (6) can be interpreted as a slip angle deficiency of the non-linear lateral force $\hat{F}_y$ from that of the linear force F_y' expected from cornering stiffness considerations, i.e., $F_y' = C_\alpha \hat{\alpha}$.

It would appear that, while we initially consider the cornering stiffness to be constant for the purpose of discussing the axle saturation approach in this paper, the validity of this assumption should depend on the vehicle/tyre characteristics. Indeed, increases in the levels of lateral acceleration lead to increases in the lateral load transfer, which, depending on the characteristics of the tyres on the vehicle, could reduce the effective cornering stiffness of an axle (Genta, 1997). For tyres that show a good degree of linearity in their cornering stiffness vs. load relations, losses in cornering stiffness at the inside tyre will be compensated by equivalent gains at the outside tyre of an axle. In this case, the axle cornering stiffness would remain fairly constant independent of the load transfer. The vehicle tyres considered for the present study satisfy this linearity assumption (and therefore, that of the constant per-axle cornering stiffness assumption made above) rather well. However, it is conceivable that a vehicle with a tyre exhibiting a higher degree of non-linearity in the cornering stiffness vs. load relation may be very sensitive to this assumption embedded in the control strategy to be proposed here. In any case, for a real-world implementation of the control strategy, an online axle cornering stiffness estimation scheme may be adopted (Sierra et al., 2006). This latter aspect is beyond the scope of this paper.

3 Axle saturation balancing control

3.1 Motivation and interpretation

It is important to note that the saturation of the front and rear axles may occur at different rates and magnitudes. This difference in the saturation levels provides a direct indication of the occurrence of understeer and oversteer behaviour for the vehicle. For example, when the front axle saturation is larger than the rear axle saturation ($\alpha_{satF} > \alpha_{satR}$) the vehicle is experiencing more understeer. This case is illustrated in Figure 3. Conversely, a more oversteering vehicle can be observed as the rear axle saturates more than the front ($\alpha_{satF} < \alpha_{satR}$). Ideally, equal saturation of the front and rear axles avoids excessive under or oversteer for the vehicle. To demonstrate this, the geometric equation representing the cornering of a single track vehicle can be used (Genta, 1997; Gillespie, 1992; Milliken, 1995; Wong, 1993).

$$\delta = \frac{L}{R} + (\alpha_F - \alpha_R) \tag{7}$$

Substituting equation (6) into equation (7):

$$(\alpha_F - \alpha_R) \cong \left(\alpha_{satF} + \frac{\hat{F}_{y,F}}{C_{\alpha,F}}\right) - \left(\alpha_{satR} + \frac{\hat{F}_{y,R}}{C_{\alpha,R}}\right) = (\alpha_{satF} - \alpha_{satR}) + \left(\frac{\hat{F}_{y,F}}{C_{\alpha,F}} - \frac{\hat{F}_{y,R}}{C_{\alpha,R}}\right) \tag{8}$$

Figure 3 Understeering vehicle axle force saturation (see online version for colours)

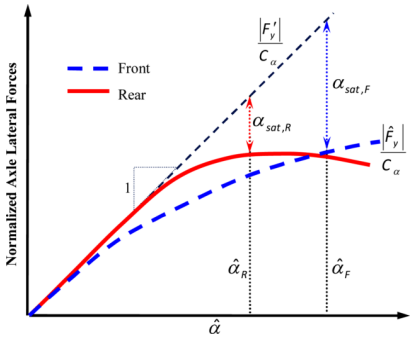

From the illustration in Figure 3, the assumption of a linear tyre for computing the slip angles α_F and α_R would have resulted in:

$$\underbrace{(\alpha_F - \alpha_R)}_{\text{Linear tire}} = \underbrace{\frac{F'_{y,F}}{C_{\alpha,F}} - \frac{F'_{y,R}}{C_{\alpha,R}}}_{\text{Linear tire}} \tag{9}$$

Comparing equations (8) and (9), it can be seen that minimising the differences in the saturation levels would leave a more linear behaviour for the differences in axle slip angles. This suggests the possibility of using the differences in axle saturation levels (axle saturation differential) for feedback control with the goal of reducing slip angle differentials between the axles. If the front/rear axle saturation level differential is kept

near zero, then it may be expected that a vehicle with non-linear tyres can be made to behave like one with linear tyres. The extent of the saturation level differential may be used by a saturation- balancing controller to identify occurrences of non-linearity and take appropriate actions to approximate the desirable predictability of a linear response as best as possible. Linear response is expected and easily perceived by most drivers.

Unlike in previous research, where axle saturation was largely considered an undesirable behaviour to be avoided through controller intervention (Limroth, 2009), the above derivation suggests that per-axle saturation can be managed through a rebalancing of saturation levels to facilitate predictability of the response and in so doing achieve stability and safety without degrading driver intentions. It is also possible that this saturation balancing approach leads to more efficient use of the tyres (and possibly the drive/actuation system) by redirecting actuation efforts to the responsive axles/tyres. In other words, it attempts to use each axle to its capacity.

3.2 Implementation of saturation balancing control

In this section, a VSC strategy employing axle saturation information is outlined. The proposed process is summarised in Figure 4. First, the axle lateral force capacity, axle slip angles and the axle saturation levels are estimated online as described in Section 2 from available vehicle dynamics sensors. These saturation levels can then be used to determine the required corrective yaw moment to minimise the axle saturation differential. As discussed earlier, there exist many activation systems including brake-based, torque vectoring, independent drive, or active steer systems that may be used to generate the corrective yaw moment on the vehicle. In the present work, the required yaw moment will be achieved by biasing the drive torque distribution between the front and rear axles in such a way as to re-balance the axle saturation levels.

Figure 4 Implementation of the saturation balancing control scheme (see online version for colours)

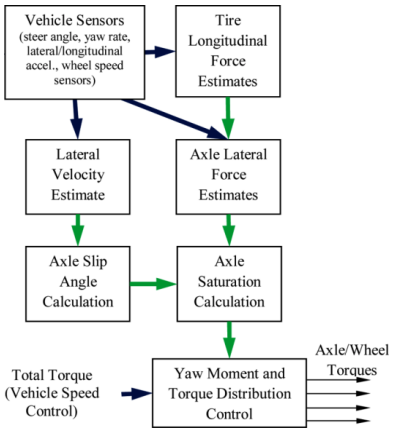

There are many possible feedback control structures that may use the axle saturation differential for VSC including PID forms, sliding mode, fuzzy-logic, or optimal controllers. Here, as an example, the corrective yaw moment may be defined by a PID form using the difference between the front/rear axle saturation levels:

$$M_{\psi} = \left(K_P + \frac{K_I}{s} + K_D s \right) (\alpha_{\text{satF}} - \alpha_{\text{satR}}) \tag{10}$$

It should be noted that this saturation-balancing controller does not need an explicit reference model to generate a desired/target response. It turns out that this control law may be given interpretations by comparing it with the common yaw rate error-based VSC systems that generate the corrective yaw moment as (Tseng et al., 1999; Zanten, 2000):

$$M'_{\psi} = \left(K'_P + \frac{K'_I}{s} + K'_D s \right) (\dot{\psi} - \dot{\psi}_{\text{desired}}) \tag{11}$$

where, $\dot{\psi}_{\text{desired}}$ is a desired yaw rate generated from a reference model. It is often taken to be the steady-state yaw rate from a linear bicycle model at speed V_x and steering input δ. It is given by:

$$\dot{\psi}_{\text{desired}} = \frac{V_x \delta}{L + (K_{\text{us}} V_x^{\,2})/g} \tag{12}$$

K_{us} is the understeer gradient computed from the axle cornering stiffness and vehicle CG locations (Gillespie, 1992).

There is a key difference between the two VSC forms equations (10) and (11) when it comes to practical implementation. The implementation of the yaw rate error control equation (11) often requires enforcing limitations for the maximum allowable (desired) yaw rate that bounds the otherwise unbounded desired yaw rate obtained from the linear steady state model ($\dot{\psi}_{\text{desired}}$). We now show that the axle saturation-balancing approach enforces an internal limit that is based on the online estimated capability of the non-linear tyres. Substituting equations (4–5) into equation (6), the front/rear axle saturation differential is given by:

$$\begin{aligned} (\alpha_{\text{satF}} - \alpha_{\text{satR}}) &= \left(\hat{\alpha}_F - \frac{\hat{F}_{y,F}}{C_{\alpha,F}} \right) - \left(\hat{\alpha}_R - \frac{\hat{F}_{y,R}}{C_{\alpha,R}} \right) \\ &= \tan^{-1}\left(\frac{\hat{V}_y + l_f \dot{\psi}}{V_x} \right) - \delta - \frac{\hat{F}_{y,F}}{C_{\alpha,F}} - \tan^{-1}\left(\frac{\hat{V}_y - l_r \dot{\psi}}{V_x} \right) + \frac{\hat{F}_{y,R}}{C_{\alpha,R}} \end{aligned} \tag{13}$$

Considering small angles (order of 10 degrees), this reduces to:

$$(\alpha_{\text{satF}} - \alpha_{\text{satR}}) \approx \frac{L\dot{\psi}}{V_x} - \left(\delta + \frac{\hat{F}_{y,F}}{C_{\alpha,F}} - \frac{\hat{F}_{y,R}}{C_{\alpha,R}} \right) \tag{14}$$

By analogy with the yaw rate error used in equation (11), we can define an 'equivalent' desired yaw rate that is implicit in the saturation balancing controller in equation (10) as:

$$\dot{\psi}'_{\text{desired}} = \left(\delta + \frac{\hat{F}_{y,F}}{C_{\alpha,F}} - \frac{\hat{F}_{y,R}}{C_{\alpha,R}} \right) \frac{V_x}{L} \tag{15}$$

This shows that the saturation balancing approach internalises the computation of a desired yaw rate, which is inherently related to the prevailing non-linear force estimates. No explicit limitation of the desired yaw rate would be required in this case.

The 'equivalent' desired yaw rate can also be given a value associated with the lateral force coefficient. Substituting $\hat{F}_y = \mu_y F_z$ in equation (14), where F_z is the axle normal load:

$$\dot{\psi}'_{\text{desired}} = \left(\delta + \frac{\mu_{y,F} F_{z,F}}{C_{\alpha,F}} - \frac{\mu_{y,R} F_{z,R}}{C_{\alpha,R}} \right) \frac{V_x}{L} \tag{16}$$

For the case with $\mu_{y,F} = \mu_{y,R} = \mu_y$, the 'equivalent' desired yaw can be written in terms of the understeer gradient and the force coefficient:

$$\dot{\psi}'_{\text{desired}} = (\delta + \mu_y K_{\text{us}}) \frac{V_x}{L} \tag{17}$$

The peak lateral friction coefficient is often assumed constant in controlled studies; however, variations do occur on different road surfaces and in changing weather conditions. The corrective yaw moment derived from axle saturation error (equation (10)) internally accounts for these variations by linking the equivalent desired yaw rate to the saturating behaviour of the tyres/axles. As a consequence of saturation balancing control, as the driver steer angle input increases, the 'equivalent' desired yaw rate is altered based on the available lateral friction, vehicle velocity, wheelbase and understeer gradient as given by equation (17) and illustrated in Figure 5. This is an added benefit of the axle saturation balancing control strategy, since it does not require explicit estimation of the tyre–road friction coefficient to take into account limitations from the saturating behaviour of the tyres. The inclusion of the non-linear tyre properties in the saturation-balancing controller allows for easy adaptation of the vehicle to sudden decreases in tyre–road friction coefficients or to sudden decreases in speed by internally reducing the 'equivalent' desired yaw rate.

Figure 5 'Equivalent' desired yaw rate used internally by the saturation balancing control (see online version for colours)

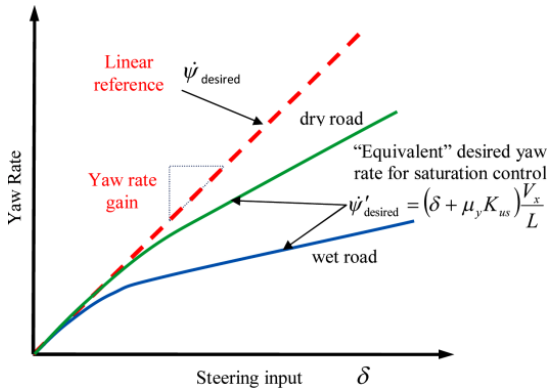

3.3 Torque biasing control

The corrective yaw moment generated via equation (10) is re-interpreted for an independent axle drive or torque-vectoring application. A torque biasing PI control can be defined from the balance of the front/rear axle saturation levels as follows:

$$\lambda = \left(K_P + \frac{K_I}{s} \right) (\alpha_{\text{satF}} - \alpha_{\text{satR}}) + \lambda_0 \tag{18}$$

And this can be compared with a torque biasing PI control that uses yaw rate error feedback:

$$\lambda = \left(K'_P + \frac{K'_I}{s} \right) (\dot{\psi} - \dot{\psi}_{\text{desired}}) + \lambda_0 \tag{19}$$

In both cases, λ is the percent of net torque to the rear axle (limited within the range of 0 and 100%), and λ_0 is the initial torque bias for which no stability control action is applied. The total torque T_{total} is computed and tuned separately so as to maintain the desired forward speed. The front and rear axle torques are given by:

$$T_F = T_{\text{total}} \times (1 - \lambda) \quad \text{and} \quad T_R = T_{\text{total}} \times \lambda. \tag{20}$$

With this torque distribution, excessive vehicle understeer, defined by more saturation on the front than rear axle, may be corrected by this controller through increased rear torque bias. Conversely, excessive oversteer is corrected through front torque bias as shown for a left turn in Figure 6 (red/dark circles indicates saturating axle/tyres).

Figure 6 Control activation for a left turn (red/dark circles indicate saturating tyres) (see online version for colours)

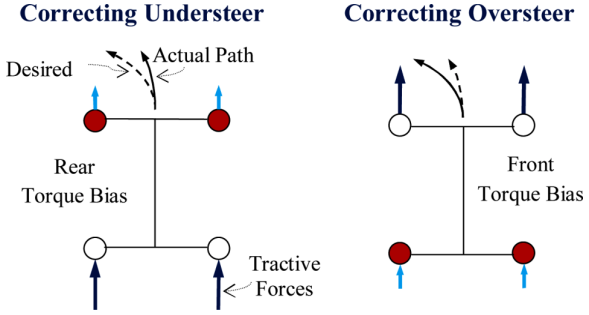

4 Results and discussions

The axle saturation balancing control method and the common yaw rate error-based stability control method were applied to simulation model of a medium duty truck with a GVW of 8000 lbs and with an upgraded power train featuring independent wheel drives. The vehicle considered is a nominally over steering vehicle with font-rear distributions of 45–45% in weight, 35–65% in initial drive and 40–60% in roll stiffness, and on dry ($\mu_{\text{peak}} = 1.0$) and wet ($\mu_{\text{peak}} = 0.6$) asphalt road. The mathematical vehicle model exercised in these analyses is the one summarised in the Appendix.

To evaluate the performance of the two stability control methods/strategies described in Section 3.3, a 'sine with dwell' steering angle input was considered as an example of an aggressive manoeuvre. This open-loop manoeuvre has been defined by NHTSA in the USA to emulate a severe obstacle avoidance type manoeuvre for evaluating VSC systems (National Highway Traffic Safety Administration (NHTSA), 2007). This input induces a dynamic non-linear vehicle response, which typically causes high vehicle sideslip for an uncontrolled vehicle. For each control strategy, the gains were tuned through trial and error by looking at the vehicle responses. For each strategy, the control gains were tuned so as to use roughly the same range of available torque-biasing/distribution within the limits of 0% and 100% on the front and rear axles.

Figure 7 shows the simulated responses of the vehicle on dry asphalt. It should be noted that the desired yaw rate shown on the plot is used only with the yaw rate error-based strategy, and is given by equation (12).

Figure 7 Response for uncontrolled and controlled vehicle on dry asphalt (μ_{peak} = 1.0) (see online version for colours)

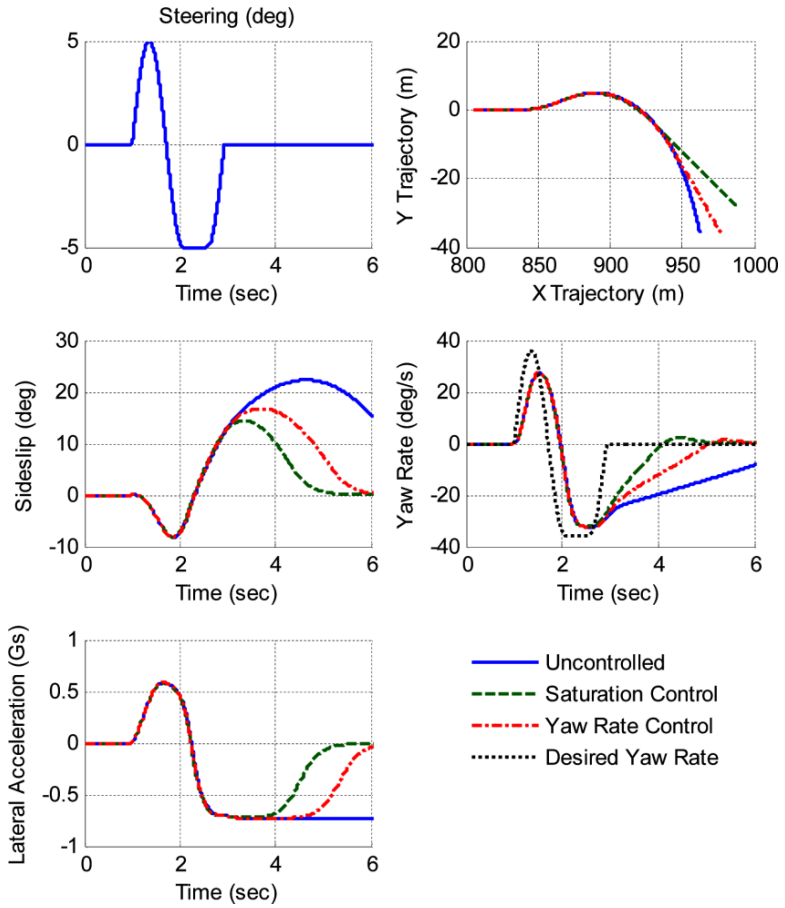

It can be seen in Figure 7 that both the saturation balancing and yaw rate error controllers reduce the sideslip of the vehicle as it concludes the manoeuvre. This can also be seen by the return of the yaw rate, side-slip angle and lateral acceleration responses to zero. The corresponding controller activity (rear torque bias) for each strategy is shown in Figure 8.

Figure 8 Yaw rate and torque bias for uncontrolled and controlled vehicle on dry asphalt (μ_{peak} = 1.0) (see online version for colours)

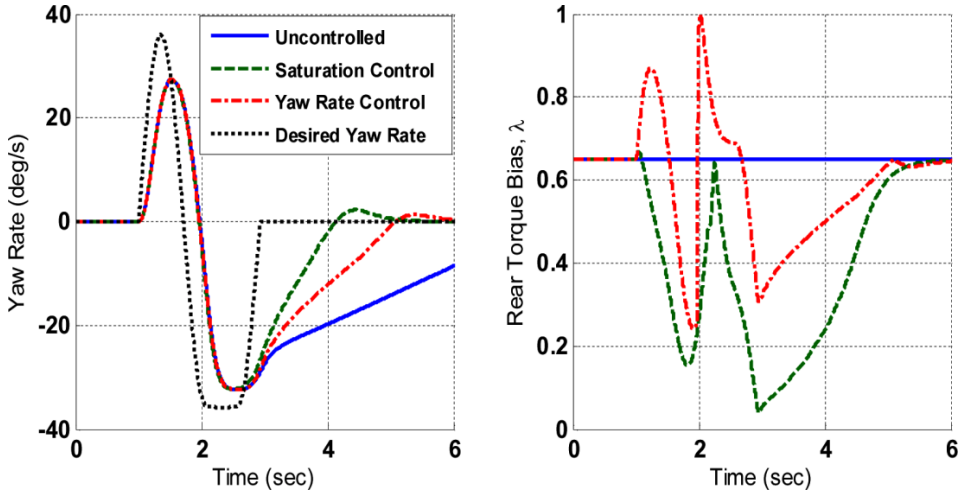

At the start of the manoeuvre, the saturation rebalancing control transfers torque-bias briefly to the rear axle but it quickly reverses the bias to the front axle (reduce rear bias), while the yaw rate control acts contrary by requesting more rear torque-bias. Since this vehicle is (nominally) slightly oversteer, the saturation-rebalancing controller seeks to balance the usage of the tyres on the front and rear axles by quickly generating a yaw moment that will induce understeer (front bias). However, the yaw rate control sees a deficiency of yaw rate from the desired (merely pre-determined from equation (12)) and acts to produce a yaw moment to increase the vehicle's yaw. These differences in activations have only small differences in their effects concerning the achievable yaw rate or trajectory of the vehicle early in the manoeuvre, but do show an impact on the different vehicle responses observed in the later more severe part of the manoeuvre involving high vehicle and tyre side slip angles.

It is known that the performance of VSC systems can be negatively affected as a vehicle transverses road surfaces of lower friction coefficients, such as wet asphalt. To evaluate the performance and effectiveness of the two VSC on such a surface, the above manoeuvre is repeated using tyre data with a peak friction coefficient of μ_{peak} = 0.6. As the manoeuvre was selected above to be extreme on dry asphalt, it is expected that the vehicle should exhibit responses with lower magnitudes on wet asphalt because of the physical tyre adhesion limits. Figure 9 shows the responses of the uncontrolled and controlled vehicle under the two controllers on wet asphalt.

Figure 9 Response for uncontrolled and controlled vehicle on wet asphalt (μ_{peak} = 0.6) (see online version for colours)

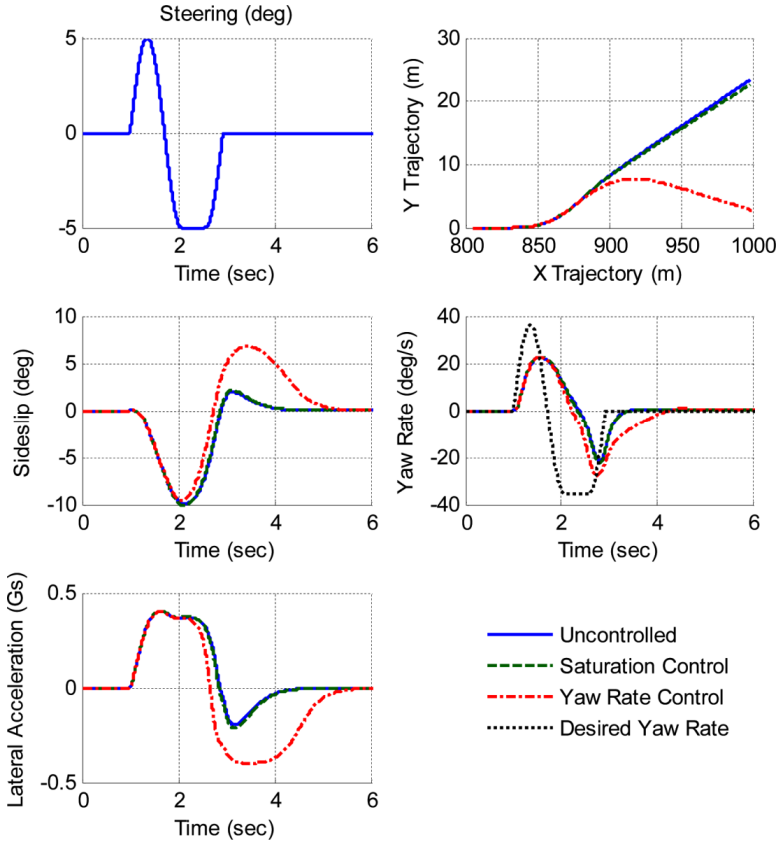

The yaw rate error control does not adapt to the lower friction coefficient but strives to track predetermined desired yaw rate, which is not limited by the severely saturating tyres on this surface. This leads to large sideslip of the vehicle for a prolonged period after the conclusion of the manoeuvre. The saturation balancing control, on the other hand, considers the reduction in lateral force capacity and limits the vehicle sideslip angle. This behaviour achieved with the saturation-balancing controller allows the vehicle to quickly recover to straight ahead at the end of the manoeuvre. The quick return of the saturation-balancing controller is very desirable from a driver's perspective and from traffic safety point of view. It means lane changes and obstacle avoidance could be executed smoothly and swiftly without alarming the driver by taking too much time in responding to his/her steering commands.

The torque-bias activations of the two stability controllers for the manoeuvre on wet asphalt are shown in Figure 10. The saturation-balancing controller achieves the observed response with lower overall swings in the torque bias except at the initial turn in. This desirable aspect can be attributed to the fact that, with the saturation-balancing controller, controller interventions are needed mainly to alleviate differences in axle saturation levels, which do not necessarily command as much torque bias as trying to track some

reference/desired yaw rate projected from a reference steady state handling model. The actual yaw rate response tracks the reference very poorly as shown in Figure 10.

Figure 10 Yaw rate and torque bias for uncontrolled and controlled vehicle on wet asphalt (μ_{peak} = 0.6) (see online version for colours)

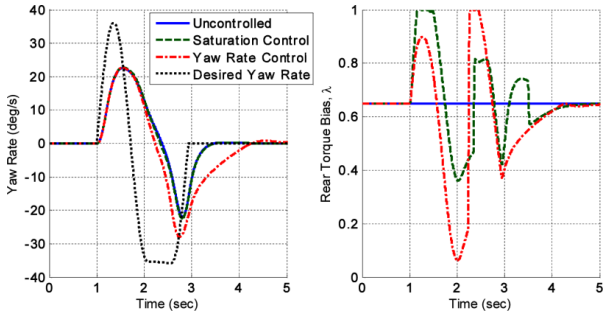

Finally, one can also look at the individual axle saturation levels during the manoeuvre to get a sense of the operating points of the two control strategies. These are shown in Figure 11 for the case of wet asphalt for the same manoeuvre considered above. It can be seen that in the latter parts of the manoeuvre the yaw rate based controller causes large axle saturation levels while the saturation-balancing controller manages these to low levels. Despite this, it should be emphasised that the saturation-balancing control strategy acts on the axle saturation differential between the front and rear axles and not on the individual axle saturation levels.

Figure 11 Front and rear axle saturations for uncontrolled and controlled vehicle on wet asphalt (μ_{peak} = 0.6) (see online version for colours)

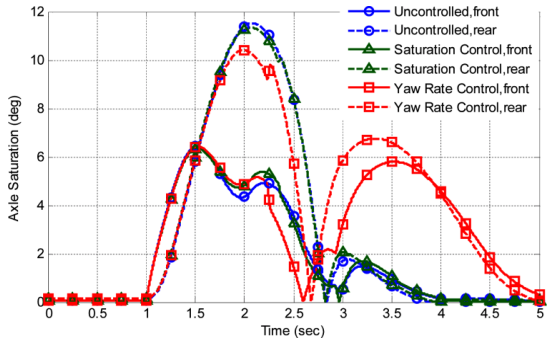

5 Conclusions

In this paper, a VSC strategy that quantifies and uses axle saturation levels is presented and compared to an established yaw rate error-based approach. The computation of the saturation levels is based on commonly available vehicle dynamics sensors and established force and slip angle estimation methods that use a 2 DOF vehicle model. The following observations are made regarding the axle saturation balancing control strategy proposed and analysed in this paper.

- The saturation-balancing control method attempts to mimic desirable linear response by minimising non-linear contributions from the saturating behaviour of the tyres on a two-axle vehicle.
- Unlike the established yaw rate error-based approaches, the saturation-balancing controller does not use an explicit reference model to generate a desired/target response. However, it is shown that the saturation-balancing control method internally uses an 'equivalent' desired or target yaw rate that takes into account the non-linear tyre force estimates. In so doing, the method also accounts for and accommodates variations in tyre–road friction without explicitly computing a friction coefficient.
- Computed axle saturation levels in an aggressive manoeuvre negotiated with the axle saturation-balancing controller and the baseline yaw rate error-based controller indicate that the former is better at managing the axle saturation levels.

6 Future Work

It has been proposed above that a per-axle saturation balancing VSC strategy may successfully stabilise and correct the course of a vehicle in destabilising situations. However, this method does not consider the capacity of individual tyres to make such corrections. The corrective wheel torques (in braking or traction) might be inadequate in conditions where the individual tyres (not axles) saturate. Therefore, it is natural to consider extending the concept of saturation balancing to a per-wheel strategy where the saturation levels will be quantified for each individual tyre. Such a per-wheel strategy would have potential benefits of reducing uneven tyre wear, through an equal usage of tyre capacity, and lowering the magnitudes of the stabilising braking/traction torques. The latter aspect may also reduce the need for activation of lower-level controllers for avoiding wheel lockup or spin.

Despite the above attractive benefits, estimation and definition of individual tyre saturation levels is not quite trivial. To define and determine individual tyre saturation levels, more detail is required in the estimations compared with what has been discussed for estimation of the axle saturation levels. While the required estimations for most of the forces and slip angles follows along the lines described above for the per-axle strategy, the slip angle estimation and lateral force estimation must be modified to separate action on the left and right tyres. The separation of lateral axle force estimation into individual left and right tyre contributions is a significant challenge that has been recognised (but not adequately solved) in previous research (Ray, 1995, 1997). It is envisioned that an appropriate tyre model may be used to separate the lumped axle lateral force estimates into contributions from the left and right side tyres. In addition, new definitions of tyre saturation levels that consider the combined longitudinal and lateral slip at each tyre are expected to enhance the possible benefit of this per-wheel saturation balancing approach. The authors expect to present results from this approach in a future publication.

Finally, we note that while the 2-DOF vehicle model assumptions were found sufficient for the per-axle force and slip angle estimations in the present simulation studies, the use of higher DOF vehicle models (including coupled roll dynamics) may

improve the determination of the saturation levels, provided the computational costs can be managed. This also constitutes a topic for future research.

Appendix: System modelling

Detailed derivations and discussions of the 7 DOF vehicle model used in this paper are given in (Karogal and Ayalew, 2009; Osborn and Shim, 2004; Genta, 1997). The notations used below are defined in the nomenclature below and in Figure 1.

The longitudinal, lateral and yaw equations of motion are, respectively:

$$\begin{aligned} m(\dot{V}_x - V_y\dot{\psi}) = \sum F_x = (F_{xLF} + F_{xRF})\cos(\delta) - (F_{yLF} + F_{yRF})\sin(\delta) \\ + F_{xLR} + F_{xRR} - \frac{1}{2}\rho C_D A V_x^{\,2} - mgC_{rr} \end{aligned} \tag{A.1}$$

$$m(\dot{V}_y + V_x\dot{\psi}) = \sum F_y = (F_{yLF} + F_{yRF})\cos(\delta) + (F_{xLF} + F_{xRF})\sin(\delta) + F_{yLR} + F_{yRR} \tag{A.2}$$

$$\begin{aligned} I_{zz}\ddot{\psi} = \sum M_z = l_f\left[(F_{yLF} + F_{yRF})\cos(\delta) + (F_{xLF} + F_{xRF})\sin(\delta)\right] + l_r(F_{yLR} + F_{yRR}) \\ + \frac{d_f}{2}\left[(F_{xRF} + F_{xLF})\cos(\delta) + (F_{yLF} - F_{yRF})\sin(\delta)\right] + \frac{d_r}{2}(F_{xRR} - F_{xLR}) \end{aligned} \tag{A.3}$$

$$\begin{aligned} I_{zz}\ddot{\psi} = \sum M_z = l_f\left[(F_{yLF} + F_{yRF})\cos(\delta) + (F_{xLF} + F_{xRF})\sin(\delta)\right] + l_r(F_{yLR} + F_{yRR}) \\ + \frac{d_f}{2}\left[(F_{xRF} + F_{xLF})\cos(\delta) + (F_{yLF} - F_{yRF})\sin(\delta)\right] + \frac{d_r}{2}(F_{xRR} - F_{xLR}) \end{aligned} \tag{A.4}$$

The tyre/wheel dynamics are given by:

$$I_w\,\dot{\omega}_i = T_{w,i} - F_{x,i}\,R_w \tag{A.5}$$

where i represents LF, RF, LR and RR tyres.

The vertical loads for the left front and left rear tyres that are required for the tyre model are given by (others follow similarly):

$$F_{zLF} = \frac{mgl_r}{2L} - A_x\left(\frac{mh_{cg}}{2L}\right) - A_y\left(\frac{ml_r h_{rcF}}{Ld_f} + \frac{m(h_{cg} - h_{rcF})K_{\varphi F}}{d_f\left(K_{\varphi F} + K_{\varphi R} - mg(h_{cg} - h_{rcF})\right)}\right) \tag{A.6}$$

$$F_{zLR} = \frac{mgl_f}{2L} + A_x\left(\frac{mh_{cg}}{2L}\right) - A_y\left(\frac{ml_f h_{rcR}}{Ld_r} + \frac{m(h_{cg} - h_{rcR})K_{\varphi R}}{d_r\left(K_{\varphi F} + K_{\varphi R} - mg(h_{cg} - h_{rcR})\right)}\right) \tag{A.7}$$

The tyre slip ratios and slip angles are computed as:

$$\kappa_i = \frac{\omega_i R_w}{V_{xi}} - 1 \tag{A.8}$$

$$\alpha_{LF} = \tan^{-1}\left(\frac{V_y + l_f\dot{\psi}}{V_x + \frac{d_f}{2}\dot{\psi}}\right) - \delta \quad \text{and} \quad \alpha_{LR} = \tan^{-1}\left(\frac{V_y - l_f\dot{\psi}}{V_x + \frac{d_f}{2}\dot{\psi}}\right) \tag{A.9}$$

Since longitudinal tractive forces of each wheel are to be exploited to influence the lateral handling dynamics, a proper tyre model that considers combined slip conditions (longitudinal and lateral) must be used, i.e., models that give $F_x = F_x(\kappa, \alpha, F_z)$ and $F_y = F_y(\kappa, \alpha, F_z)$ are needed. For this purpose, combined-slip tyre data provided in (Pacejka, 2002) was suitably scaled by tyre size/load and implemented as a multi-dimensional lookup table.

References

Esmailzadeh, E., Goodarzi, A. and Vossoughi, G.R. (2002) 'Directional stability and control of four-wheel independent drive electric vehicles', *Proc. Instn. Mech. Engrs. Part K: J. Multi-body Dynamics*, Vol. 216, No. 4, pp.303–313.

Falcone, P., Borrelli, F., Asgari, J., Tseng, H. E. and Hrovat, D. (2007) 'Predictive active steering control for autonomous vehicle systems', *Control Systems Technology*, *IEEE Transactions*, Vol. 15, No. 3, pp.566–580.

Falcone, P., Tufo, M., Borrelli, F., Asgari, J. and Tseng, H. E. (2008a) 'A linear time varying model predictive control approach to the integrated vehicle dynamics control problem in autonomous systems', *Proceedings of the 46th IEEE Conference on Decision and Control*, New Orleans, LA, pp.2980–2985.

Falcone, P. Tseng, H E., Borrelli, F., Asgari, J. and Hrovat, D. (2008b) 'MPC-based yaw and lateral stabilisation via active front steering and braking', *Vehicle System Dynamics: International Journal of Vehicle Mechanics and Mobility*, Vol. 46, No. 1, Supp. 1, pp.611–628.

Fukada, Y. (1999) 'Slip-angle estimation for vehicle stability control', *Vehicle System Dynamics: International Journal of Vehicle Mechanics and Mobility*, Vol. 32, No. 4, pp.375–388.

Genta, G. (1997) 'Motor vehicle dynamics: modeling and simulation', *Series on Advances in Mathematics for Applied Sciences*, Vol. 43, World Scientific Publishing, Singapore, pp.205–324.

Ghoneim, Y., Lin, W., Sidlosky, D., Chen, H., Chin, Y. and Tedrake, M. (2000) 'Integrated chassis control system to enhance vehicle stability,' *International Journal of Vehicle Design*, Vol. 23, pp.124–144.

Gillespie, T. (1992) *Fundamentals of Vehicle Dynamics*, Society of Automotive Engineers, Warrendale, PA.

Goodarzi, A. and Esmailzadeh, E. (2007) 'Design of a VDC system for all-wheel independent drive vehicles', *IEEE/ASME Transactions on Mechatronics*, Vol. 12, No. 6, pp.632–639.

Gradu, M. (2003) *Torque Bias Coupling for AWD Applications*, SAE Paper No. 2003-01-0676, Detroit, MI.

Hac, A. and Bodie, M. (2002) 'Improvements in vehicle handling through integrated control of chassis systems', *International Journal of Vehicle Autonomous Systems*, Vol. 1, No. 1, pp.83–110.

Hongyan, G., Hong, C. and Tonghao, S. (2009) 'Tire-road forces estimation based on sliding mode observer', *International Conference on Mechatronics and Automation*, Changchun, Jilin, China, pp.4577-4582

Karogal, I. and Ayalew, B. (2009) *Independent Torque Distribution Strategies for Vehicle Stability Control*, SAE Paper Number 2009-01-0456, Detroit, MI.

Kim, J. (2009) 'Identification of lateral tyre force dynamics using an extended Kalman filter from experimental road test data', *Control Engineering Practice*, Vol. 17, No. 3, pp.357–367.

Kim, J. (2010) 'Effect of vehicle model on the estimation of lateral vehicle dynamics', *International Journal of Automotive Technology*, Vol. 11, No. 3, pp.331–337.

Kim, J. and Kim, H. (2007) 'Electric vehicle yaw rate control using independent in-wheel motor', *IEEE*, *Power Conversion Conference*, Nagoya, Japan , pp.705–710.

Limroth, J. (2009) *Real-time Vehicle Parameter Estimation and Adaptive Stability Control*, PhD Dissertation in Automotive Engineering, Clemson University, Clemson, SC.

Milliken, W.M.A.D. (1995) *Race Car Vehicle Dynamics*, Society of Automotive Engineers, Inc., Warrendale, PA.

Mohan, S.K. and Sharma, A. (2006) *Torque Vectoring Axle and Four Wheel Steering: A Simulation Study of Two Yaw Moment Generation Mechanisms*, SAE Paper Number 2006-01-0819, Detroit, MI.

National Highway Traffic Safety Administration (NHTSA) (2007) *Federal Motor Vehicle Safety Standards; Electronic Stability Control Systems; Controls and Displays; 49 CFR Parts 571 and 585*.

Osborn, R.P. and Shim, T. (2004) *Independent Control of All-Wheel-Drive Torque Distribution*, SAE Paper Number 2004-01-2052, Detroit, MI.

Pacejka, H.B. (2002) *Tyre and Vehicle Dynamics*, Butterworth-Heinemann, Oxford.

Piyabongkarn, D., Lew, J. Y., Rajamani, R., Grogg, J. A. and Qinghui, Y (2007) 'On the use of torque-biasing systems for electronic stability control: limitations and possibilities', *IEEE Transaction on Control Systems Technology*, Vol. 15, No. 3, pp.581–589.

Rajamani, R. (2006) *Vehicle Dynamics and Control*, Springer, New York, NY.

Ray, L.R. (1995) 'Nonlinear state and tire force estimation for advanced vehicle control', *IEEE Transactions on Control Systems Technology*, Vol. 3, No. 1, pp.117–124.

Ray, L.R. (1997) 'Nonlinear tire force estimation and road friction identification: simulation and experiments', *Automatica*, Vol. 33, No. 10, pp.1819–1833.

Sierra, C., Tseng, E., Jain, A., and Peng, H. (2006) 'Cornering stiffness estimation based on vehicle lateral dynamics', *Vehicle System Dynamics: International Journal of Vehicle Mechanics and Mobility*, Vol. 44, No. 1, pp.24–38.

Tseng, H.E., Ashrafi, B., Madau, D., Allen Brown, T. and Recker, D (1999) 'The development of vehicle stability control at Ford', *Mechatronics*, *IEEE/ASME Transactions on*, Vol. 4, No. 3, pp.223–234.

Wanki, C. , Jangyeol, Y., Seongjin, Y., Bongyeong, K. and Kyongsu, Y. (2010) 'Estimation of tire forces for application to vehicle stability control', *Vehicular Technology*, *IEEE Transactions*, Vol. 59, No. 2, pp.638–649.

Wong, J.Y. (1993) *Theory of Ground Vehicles*, John Wiley & Sons, New York, NY.

Zanten, T.V. (2000) 'Bosch ESP systems: 5 years of experience', in *SAE Automotive Dynamics & Stability Conference*, SAE Paper Number 2000-01-1633, Troy, MI.

Nomenclature

α_i	Lateral slip angle of tyre *i*
$\alpha_{sat,i}$	Saturation of tyre *i*
δ	Road wheel steering angle
κ_i	Longitudinal slip of tyre *i*
ρ	Density of air

$\dot{\psi}$	Vehicle yaw rate
λ	Rear torque bias
λ_0	Initial rear torque bias
ω_i	Rotational speed of wheel i
μ	Friction coefficient
A	Vehicle frontal area
A_x, A_y	Longitudinal and lateral acceleration
$C_{\alpha,F}$, $C_{\alpha,R}$	Front/rear axle cornering stiffnesses
C_D	Drag coefficient
C_{rr}	Rolling resistance coefficient
F_x	Longitudinal tyre force
F_y	Lateral tyre force
F_z	Normal tyre load
g	Gravitational constant
h_{cg}	Vehicle CG height
h_{rcF}, h_{rcR}	Front/rear roll centre height
I_{zz}	Yaw inertia
I_w	Inertia of motor/wheel referred to wheel
$K_{\phi R}$, $K_{\phi L}$	Rear/front roll stiffness
Kp, K_I, K_D	Controller gains
L	Wheel base
l_f, l_r	Distance of front/rear axle from vehicle CG
m	Total vehicle mass
R_W	Effective wheel radius
d_f, d_r	Front/rear wheel track width
T_f, T_r	Front/rear axle torques
T_{total}	Total wheel torque
$T_{w,i}$	Individual wheel torque
V_x	Longitudinal velocity in vehicle x-axis
V_y	Lateral velocity in vehicle y-axis